COMMUNICATION

Reaction Rate Inside the Cavity of $[Ga_4L_6]^{12-}$ Supramolecular Metallocage is Regulated by the Encapsulated Solvent

Gantulga Norjmaa, Jean-Didier Maréchal* and Gregori Ujaque*[a]

**Abstract:** In the present study the dependence of the reaction rate of carbon-carbon reductive elimination from $R_3PAu(MeOH)(CH_3)_2$ complexes inside $[Ga_4L_6]^{12-}$ metallocage on the nature of the phosphine ligand is investigated by computational means. The reductive elimination mechanism is analyzed in methanol solution and inside the metallocage. Classical molecular dynamics simulations reveal that the smaller the gold complex (which depends on the phosphine ligand size) the larger the number of solvent molecules encapsulated. The size of the phosphine ligands defines the space that is left available inside the cavity that can be occupied by solvent molecules. The Gibbs energy barriers calculated at DFT level, in excellent agreement with experiment both in solution and in the metallocage, show that the presence/absence of explicit solvent molecules inside the cavity significantly modifies the reaction rate.

Supramolecular catalysis is a very rapid expanding discipline that joins catalysis and supramolecular chemistry.[1–8] Several supramolecular hosts have been designed as nanoreactors and applied to the host-guest catalysis, with metallocages playing a prominent role.[9–12] Metallocages (M_xL_y) are synthesized from metal ions and organic ligands (linkers) and offer well defined cavities in size and shape to host molecules and chemical reactions.[13,14] Examples include Raymond's Ga_4L_6,[15] Fujita's Pd_6L_4,[16] Nitschke's Fe_4L_6,[17] Lusby's Pd_2L_4,[18] among others.[19,20]

The tetrahedron supramolecular metallocage, $K_{12}[Ga_4L_6]$, developed by Raymond and coworkers, has been applied to many reactions as the C-C reductive elimination from Au(III) and Pt(IV) complexes,[21] the orthoformate hydrolysis,[22] Nazarov cyclization,[23] the hydroalkylation,[24] etc.[25–27] The great catalytic power of the metallocage, $[Ga_4L_6]^{12-}$, for the C-C reductive elimination has been studied in detail by Bergman, Raymond and Toste.[21,28] One of the most interesting findings regarding the relationship between the metallocage and the hosted catalytic system is related to the dependence of the catalytic kinetics in function of the nature of the phosphine ligand. Indeed, the presence of PEt_3 vs. PMe_3 as gold ligand significantly influences the Gibbs energy barrier of the reductive elimination inside the

metallocage, but not in solution. The ratio between measured Michaelis-Menten rate constants, $k_{cat}(PEt_3)/ k_{cat}(PMe_3)$, is calculated to be 103, whereas the ratio between observed uncatalyzed rate constants, $k_{uncat}(PEt_3)/ k_{uncat}(PMe_3)$, is around 2.7 (Scheme 1). Understanding the origin of such a different behavior is a challenge from both chemical and computational point of view but could lead to major improvement in developing novel metallocages and/or looking for new guest reactions.

Theoretical analysis are key for understanding catalysis;[29–31] though computational studies on supramolecular catalysis are still scarce.[32–39] In the case of highly charged hosts, as the $[Ga_4L_6]^{12-}$ metallocage, all theoretical investigations indicate that electrostatic effects are essential for the rate acceleration.[40–43] In our previous study, we showed that not only encapsulation by the host, but also microsolvation is important for lowering the Gibbs energy barrier of the reductive elimination from the cationic Au(III) complex, $R_3PAu(MeOH)(CH_3)_2$, inside $[Ga_4L_6]^{12-}$.[43] We here investigate computationally the origin of the different catalytic behavior observed experimentally for C-C reductive elimination using PEt_3 and PMe_3 as ligands for the same gold complex (Scheme 1).
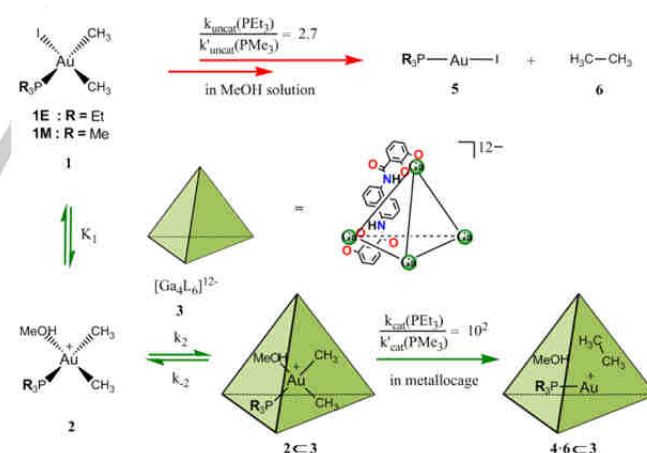
Scheme 1. Schematic representation of reductive elimination from $[(R_3P)Au(I)(CH_3)_2]$ complex, **1**. Reaction in MeOH solution (red arrow) and within $[Ga_4L_6]^{12-}$ metallocage **3**, (green arrow). **1M**: R=Me; **1E**: R=Et.

The C-C reductive elimination reaction is evaluated computationally for $[Me_3PAu(I)(CH_3)_2]$ **1M** as starting reactant in MeOH solution (Scheme 1) including the first solvation shell explicitly (12 MeOH molecules; Figure 1 black profile).[44] Assuming the formation of the cationic species **2M-12** $([Me_3PAu(MeOH)(CH_3)_2]^+)$ the calculated Gibbs energy barrier is 26.2 kcal/mol (Figure 1), in excellent agreement with the estimated value of 27.2 kcal/mol obtained experimentally from

[a]   G. Norjmaa, Dr. JD. Maréchal, Dr. G. Ujaque
        Departament de Química and Centro de Innovación en Química
        Avanzada (ORFEO-CINQA)
        Universitat Autònoma de Barcelona
        08193 Cerdanyola del Valles, Barcelona, Catalonia, Spain
        E-mail: jeandidier.marechal@uab.cat, gregori.ujaque@uab.cat

the measured rate constant of $6.6 \cdot 10^{-8}$ s^{-1} at 298K.[21] In the transition state, **TS_2M-12**, the forming C-C bond distance is 2.176 Å. For comparison, the results for complex **2E** with PEt$_3$ lead to a Gibbs energy barrier is 25.0 kcal/mol,[43] **TS_2E-12**, also in very good agreement with the experimental value of 26.7 kcal/mol. Therefore, the difference in calculated Gibbs energy barriers for gold complexes with PMe$_3$ and PEt$_3$ ligands in solution is 1.2 kcal/mol (26.2 kcal/mol vs 25.0 kcal/mol, from the starting gold complexes) which is also close to the experimental difference of 0.5 kcal/mol (Figure S4b). Interestingly, the forming C-C bond distances in the transition states are very similar, 2.176 Å and 2.177 Å for gold complexes with PMe$_3$ and PEt$_3$ ligands, respectively.

So far the study clearly indicates that electronic effects of the phosphine ligand does not have major contribution in the difference observed in the rate acceleration. Following on the previous findings on the PEt$_3$ system, we focused on microsolvation effects. To evaluate them two additional models for the complex with PMe$_3$, including one or two explicit MeOH molecules, **2M** and **2M-2**, were considered. In these cases, the Gibbs energy barrier diminishes to 21.0 and 23.7 kcal/mol, respectively. These results are analogous from those of our previous study for complex **2E** (Figure S4b):[43] removing explicit solvent MeOH molecules around the cationic gold complex decreases the Gibbs energy barrier of the reductive elimination.

To proceed with the study of the encapsulated reaction we performed first classical molecular dynamics (MD) simulations of the gold complex inside metallocage **3**.[44] Calculations were carried out within a periodic box of explicit solvent MeOH molecules. Two systems were evaluated: (i) **2M⊂3** containing the square planar gold complex, **2M**, encapsulated in the metallocage **3**, and (ii) **1M-I⊂3** containing a T-shaped gold complex, **1M-I**, encapsulated in the metallocage **3**. Because of the relevance of the solvent environment identified in the first part of the study, the occupancy of methanol molecules into the cage was first analysed. Both systems show that there are two solvent MeOH molecules in the cavity of the metallocage along with the gold complex during the simulation time (over 100 ns; Figure S1). Statistical analysis of the cavity size of the free or loaded metallocages from the MD simulations show that its weighted average volume is 429 ± 84.8 Å^3 independently of its loaded state (see Table S1). These results point out that the relevant models should account with two solvent MeOH molecules inside the metallocage.

Based on the molecular dynamics simulations, the reductive elimination process inside the metallocage was computed at DFT level using the system **2M-2⊂3** (a model that includes the gold complex, two solvent MeOH molecules with one coordinated, and the [Ga$_4$L$_6$]$^{12-}$ metallocage **3**).[44] The Gibbs energy barrier is 20.7 kcal/mol (Figure 1, green profile), quite close to the estimated value of 19.5 kcal/mol from the experimental rate constant of $3.3 \cdot 10^{-2}$ s^{-1} at 298K.[21] The forming C-C bond distance in transition state, **TS_2M-2⊂3**, is 2.174 Å is very similar to that in solution, 2.176 Å, for **TS_2M-12**. This shows that the geometry of the transition state is not significantly affected by encapsulation. Importantly, the analysis for the encapsulated gold complex with PEt$_3$, **2E⊂3**, showed that no additional solvent molecules (apart from the coordinated one) are present inside the cavity. The calculated barrier is 15.5 kcal/mol is quite close to 16.7 kcal/mol value estimated from the experimental rate constant of 3.4 s^{-1}.[21] Both Gibbs energy barriers are in very good agreement with experiment and the comparison between these two processes gives a $\Delta\Delta G^{\ddagger}$ of 5.2 kcal/mol also in good agreement with observed experimental value of ca. 3.0 kcal/mol.

In order to analyze microsolvation and encapsulation effects for **2M-2** system (containing PMe$_3$), the reaction can be formally described in two hypothetic processes: (i) removing explicit microsolvation around the gold complex (until there are only two solvent molecules, **2M-2**; from black to purple profiles in Figure 1) and (ii) encapsulating this system into the metallocage (from purple to green profile in Figure 1). The first process diminishes the barrier by 0.7 kcal/mol, whereas the second decreases the barrier by 3.0 kcal/mol for **2M-2** (Figure S6). The effect of microsolvation and encapsulation for **2E** (containing PEt$_3$) were found to be diminishing the barrier by 5.7 and 3.1 kcal/mol, respectively.[43] The main difference comes from the microsolvation process: in **2M-2**, the gold complex (with PMe$_3$) is surrounded by two MeOH solvent molecules (one coordinated and one not) whereas in **2E** the gold complex (with PEt$_3$) contains only one (the one coordinated). According to the calculated barriers the presence of the second MeOH solvent molecule for the complex with the smaller phosphine ligand has a decisive role in hampering the reaction.

So far, our study points out that the difference in microsolvation between **2M⊂3** and **2E⊂3** is likely to be the main responsible of the change in acceleration rate observed experimentally. We decided to investigate further the origin and the impact of such changes in the solvation profiles. First a series of calculations were carried out on **2M⊂3**; a system where the square-planar gold complex **2M** inside the metallocage has no additional solvent molecules apart from the coordinated one (Figure S3). When comparing **2M⊂3**, and **2M-2⊂3**, it appears that:

 (i) DFT optimized systems show that the Gibbs energy barrier decreases from 20.7 kcal/mol for **2M-2⊂3** (Figure S5) to 13.0 kcal/mol for **2M⊂3**. The Gibbs energy barrier diminishes by removing a surrounding solvent molecule from the cavity which indicates that the presence of solvent inside the metallocage significantly influences the barrier and confirming the importance of microsolvation.
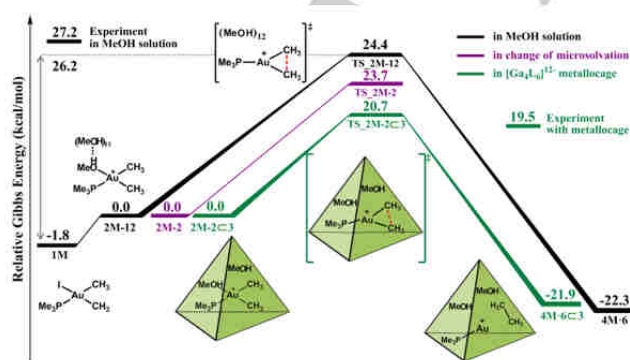
(ii) Despite **2M⊂3** shows lower transition state barriers than **2M-2⊂3**, the latter provides with the closest value to the experiment[45]. Similar behavior was found when comparing energy barriers for the gold system with PEt₃, (**2E⊂3** vs. **2E-2⊂3**; 15.4 kcal/mol vs. 19.7 kcal/mol, respectively). The lower computed barriers correspond to processes where the reactant disposition (**2M⊂3**) is hardly reachable in this solvent according to MD analysis. However, a more realistic description of the reactant inside the metallocage (**2M-2⊂3**) gives a closer energy barrier compared to the experiment (16.7 kcal/mol). This highlights that the experimental behaviors observed for **2E** and **2M** encapsulated systems in **3** can be explained on the basis of different numbers of solvent molecules in the cavity.

(iii) C-C bond distance for **TS_2M⊂3** of 2.161 Å is only slightly shortened compared to that for **TS_2M-2⊂3**, 2.176 Å. This shows that there is structurally little constraints on the transition state structure in function of the number of solvent molecules (Figure S2).

(iv) All the DFT optimized structures of the entire study show cavities that are within 300-500 Å³ range, in agreement with MD simulations. For **TS_2M⊂3** the volume falls down to 237 Å³; a value quite far from what appear in room temperature and bulk conditions. Further analysis of the structure of the cage actually shows a substantial packing of the cage upon removal of the solvent molecule in the transition state.

Taken all those data together brings a better understanding of the molecular grounds of the difference in rate acceleration of **2M⊂3** and **2E⊂3** particularly on the origin of the number of solvent molecules in and its real impact on the mechanism. The cavity of the cage has under room temperature conditions a volume that allows to host one (**2E**) or two (**2M**) solvent molecules. For the former, this molecule coordinates the metal in the reactant form and leaves in the transition state although remaining in the vicinity of the catalytic metal. For the latter, one molecule coordinates while the other remains in the cavity in the reactant state and in the transition state both solvent molecules remain in the cavity. Overall any alteration of the microsolvation should lead to differences in the experimental behaviors. The size of the accessible host cavity to embed guests (being catalysts, substrate(s) and solvent molecule(s)), has also a major contribution on the reactive profiles; the number of encapsulated solvent molecules is function of the phosphine ligand. This study confirms that the presence of non coordinating ones is crucial for the process as our previous study implied. The role assigned to coordinated and surrounding solvent molecules in this work differ from other recently published works where they propose that the complexed water also serves as a strong catalytic player.[46]

In conclusion, this study highlights that the main difference on the rate enhancement upon encapsulation in [Ga₄L₆] of the Au(III) complexes, R₃PAu(MeOH)(CH₃)₂ in function of the phosphine ligands R (PEt₃ vs PMe₃) is unambiguously related to a combination of factors where predominate the accessible cavity size and the availability to accommodate additional solvent MeOH molecules surrounding the gold complex inside the cavity. Whereas for the gold complex with the PEt₃ ligand (**2E⊂3**) there are no additional solvent MeOH molecules within the cavity of the metallocage except the one coordinated to the metal, for the gold complex with PMe₃ ligand (**2M⊂3)** there is a second non coordinated MeOH molecule inside the cavity that causes a decrease in the reaction rate. The size of the gold complex as well as the size of the same cavity govern the space availability to accommodate additional MeOH solvent molecules, and the presence/absence of these solvent molecules modifies the reaction rate for the process. This evidences that size matters in encapsulated metallocage catalysis and that the improvement of the catalytic profile of encapsulated catalysis is far from a "simple" result of the incorporation of the reactive complex in the cage but a fine balance in the interplay between host, guest and solvent molecules. Size, shape, solvent accessibility, and modularity of the cage dimension are magnitudes that contribute to the rate acceleration. Understanding and foreseeing these elements, eventually throughout computational means, could be in the rational design of host-guest catalysis.

Acknowledgements

[1] Y. Fang, J. A. Powell, E. Li, Q. Wang, Z. Perry, A. Kirchon, X. Yang, Z. Xiao, C. Zhu, L. Zhang, F. Huang, H.-C. Zhou, *Chem. Soc. Rev.* **2019**, *48*, 4707–4730.

[2] L. Zhao, X. Jing, X. Li, X. Guo, L. Zeng, C. He, C. Duan, *Coord. Chem. Rev.* **2019**, *378*, 151–187.

[3] P. Ballester, A. Scarso, *Front. Chem.* **2019**, *7*, 174.

[4] C. Tan, D. Chu, X. Tang, Y. Liu, W. Xuan, Y. Cui, *Chem. Eur. J.* **2019**, *25*, 662–672.

[5] Q. Zhang, L. Catti, K. Tiefenbacher, *Acc. Chem. Res.* **2018**, *51*, 2107–2114.

[6] C. Deraedt, D. Astruc, *Coord. Chem. Rev.* **2016**, *324*, 106–122.

[7] W. Cullen, M. C. Misuraca, C. A. Hunter, N. H. Williams, M. D. Ward, *Nat. Chem.* **2016**, *8*, 231–236.

[8] S. H. A. M. Leenders, R. Gramage-Doria, B. De Bruin, J. N. H. Reek, *Chem. Soc. Rev.* **2015**, *44*, 433–448.

[9] S. Datta, M. L. Saha, P. J. Stang, *Acc. Chem. Res.* **2018**, *51*, 2047–2063.

[10] S. Pullen, G. H. Clever, *Acc. Chem. Res.* **2018**, *51*, 3052–3064.

[11] C. J. Brown, F. D. Toste, R. G. Bergman, K. N. Raymond, *Chem. Rev.* **2015**, *115*, 3012–3035.

[12] H. Amouri, C. Desmarets, J. Moussa, *Chem. Rev.* **2012**, *112*, 2015–2041.

[13] C. M. Hong, R. G. Bergman, K. N. Raymond, F. D. Toste, *Acc. Chem. Res.* **2018**, *51*, 2447–2455.

[14] H. Vardhan, F. Verpoort, *Adv. Synth. Catal.* **2015**, *357*, 1351–1368.

[15] J. A. Leary, C. Brückner, K. N. Raymond, D. L. Caulder, T. N. Parac, S. König, R. E. Powers, *J. Am. Chem. Soc.* **2002**, *123*, 8923–8938.

[16] M. Yoshizawa, M. Tamura, M. Fujita, *Science.* **2006**, *312*, 251–255.

[17] J. L. Bolliger, A. M. Belenguer, J. R. Nitschke, *Angew. Chemie. Int. Ed.* **2013**, *52*, 7958–7962.

[18] V. Martí-Centelles, A. L. Lawrence, P. J. Lusby, *J. Am. Chem. Soc.* **2018**, *140*, 2862–2868.

[19] C. García-Simón, R. Gramage-Doria, S. Raoufmoghaddam, T. Parella, M. Costas, X. Ribas, J. N. H. Reek, *J. Am. Chem. Soc.* **2015**, *137*, 2680–2687.

[20] Z. Lu, R. Lavendomme, O. Burghaus, J. R. Nitschke, *Angew. Chemie. Int. Ed.* **2019**, *58*, 9073–9077.

[21] D. M. Kaphan, M. D. Levin, R. G. Bergman, K. N. Raymond, F. D. Toste, *Science.* **2015**, *350*, 1235–1238.

[22] M. D. Pluth, R. G. Bergman, K. N. Raymond, *Science.* **2007**, *316*, 85–88.

[23] C. J. Hastings, M. D. Pluth, R. G. Bergman, K. N. Raymond, *J. Am. Chem. Soc.* **2010**, *132*, 6938–6940.

[24] Z. J. Wang, C. J. Brown, R. G. Bergman, K. N. Raymond, F. D. Toste, *J. Am. Chem. Soc.* **2011**, *133*, 7358–7360.

[25] C. J. Brown, R. G. Bergman, K. N. Raymond, *J. Am. Chem. Soc.* **2009**, *131*, 17530–17531.

[26] D. H. Leung, R. G. Bergman, K. N. Raymond, *J. Am. Chem. Soc.* **2006**, *128*, 9781–9797.

[27] D. H. Leung, R. G. Bergman, K. N. Raymond, *J. Am. Chem. Soc.* **2007**, *129*, 2746–2747.

[28] M. D. Levin, D. M. Kaphan, C. M. Hong, R. G. Bergman, K. N. Raymond, F. D. Toste, *J. Am. Chem. Soc.* **2016**, *138*, 9682–9693.

[29] K. N. Houk, *Chem. Soc. Rev.* **2014**, *43*, 4905.

[30] D. J. Tantillo, *Acc. Chem. Res.* **2016**, *49*, 1079–1079.

[31] J. N. Harvey, F. Himo, F. Maseras, L. Perrin, *ACS Catal.* **2019**, *9*, 6803–6813.

[32] P. Carlqvist, F. Maseras, *Chem. Commun.* **2007**, 748–750.

[33] S. P. Kim, A. G. Leach, K. N. Houk, *J. Org. Chem.* **2002**, *67*, 4250–4260.

[34] C. Goehry, M. Besora, F. Maseras, *ACS Catal.* **2015**, *5*, 2445–2451.

[35] H. Daver, J. N. Harvey, J. Rebek, F. Himo, *J. Am. Chem. Soc.* **2017**, *139*, 15494–15503.

[36] C. Goehry, M. Besora, F. Maseras, *European J. Org. Chem.* **2018**, 2103–2109.

[37] D. Chakraborty, P. K. Chattaraj, *J. Comput. Chem.* **2018**, *39*, 151–160.

[38] E. Pahima, Q. Zhang, K. Tiefenbacher, D. T. Major, *J. Am. Chem. Soc.* **2019**, *141*, 6234–6246.

[39] T. A. Young, V. Martí-Centelles, J. Wang, P. J. Lusby, F. Duarte, *J. Am. Chem. Soc.* **2020**, *142*, 1300-1310.

[40] V. Vaissier Welborn, T. Head-Gordon, *J. Phys. Chem. Lett.* **2018**, *9*, 3814–3818.

[41] M. P. Frushicheva, S. Mukherjee, A. Warshel, *J. Phys. Chem. B* **2012**, *116*, 13353–13360.

[42] K. Wang, X. Cai, W. Yao, D. Tang, R. Kataria, H. S. Ashbaugh, L. D. Byers, B. C. Gibb, *J. Am. Chem. Soc.* **2019**, *141*, 6740–6747.

[43] G. Norjmaa, J.-D. Maréchal, G. Ujaque, *J. Am. Chem. Soc.* **2019**, *141*, 13114–13123.

[44] DFT calculations were performed with Gaussian09 at B3LYP-D3 level. MD calculations wiere carried out with AMBER. See Supporting Information for Computational Details.

[45] Possible other configurations of encapsulated reactants and transition state were also optimized and geometries are shown in Figure S3. Those configurations are calculated to be more than 4.0 kcal/mol higher in Gibbs energy than the ones commented in the main text.

[46] V. V. Welborn, W. Li, T. Head-Gordon, *Nat Commun.* **2020**, *11*, 415.

Entry for the Table of Contents (Please choose one layout)

Layout 1:

COMMUNICATION

The reductive elimination process for $R_3PAu(MeOH)(CH_3)_2$ complexes are investigated in MeOH solution and inside the $[Ga_4L_6]^{12-}$ metallocage. The size of the metal complex and the size of the cavity govern the space availability to accommodate additional MeOH solvent molecules. Reaction rate is regulated by the presence/absence of these solvent molecules.
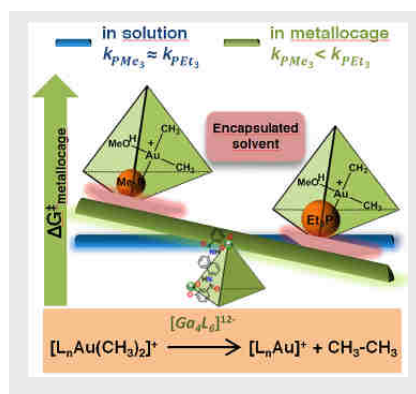
G. Norjmaa, JD. Maréchal*, G. Ujaque*

Page No. – Page No.

Reaction Rate Inside the Cavity of $[Ga_4L_6]^{12-}$ Supramolecular Metallocage is Regulated by the Encapsulated Solvent

Layout 2:

COMMUNICATION

((Insert TOC Graphic here))

Author(s), Corresponding Author(s)*

Page No. – Page No.

Title

Text for Table of Contents